Structure and optical properties of spin coated $Zn_{0.9}M_{0.1}O$ (M: Cd, Mg) nanostructured films as transparent electrodes

AMRITPAL SINGH, PRAVEEN KUMAR[a,*]
Nanotechnology Research Centre, DAV Institute of Engineering and Technology, Kabir Nagar, Jalandhar-144008, India
[a]Department of Physics, DAV University, Sarmastpur, Jalandhar-144012, India

The present work reports the effect of (Cd, Mg) doping on the optical and electrical properties of the zinc oxide for their probable application as transparent electrodes in modern display devices and organic solar cells. The effect of Cd and Mg incorporation on the structure, optical and electrical properties of sol gel synthesized ZnO films by X-ray diffraction, atomic force microscopy, UV-Vis spectroscopy, photoluminescence and electrical measurements. The X-ray diffraction study has revealed the hexagonal wurtzite crystal structure having preferential c-axis orientation for the Mg doped samples. The improvement in surface roughness with the decrease in the grain size has been observed for the Mg doped ZnO films. The formation of highly transparent films (>86%) along with the increase in the optical gap for the Mg doped films has been observed. The photoluminescence measurements revels the decrease in the defects for the Mg dopant as compared to the Cd in the ZnO films. The higher value of the optical transparency and electrical resistivity for the Mg doped samples will make them suitable for their application as transparent electrodes.

(Received April 8, 2013; accepted March 13, 2014)

Keywords: Transparent conductors, Spin coating; XRD, UV–Vis spectroscopy, Fluorescence spectroscopy

1. Introduction

Transparent conducting oxides having a wide band-gap (>3.0eV) are being used extensively for photovoltaic and optoelectronic devices. Among these materials, zinc oxide (ZnO) is a promising material for novel device applications such as transparent electronics, flexible displays, piezoelectric transducers, surface acoustic wave (SAW) devices, laser diodes, photoconductive UV detectors and gas sensors etc. due to its unique optical and electrical properties [1-3]. ZnO is also commercially available with advantages such as comparatively low cost, non-toxic environment-friendly nature, high thermal stability, high resisting to radiation damage and chemically stable. The physical characteristics of ZnO can be successfully optimized by doping as well as optimizing the various processing conditions [remove these references 4-10]. ZnO has been successfully doped with a number of elements i.e. Cd, Al, Mg, Sn, In, V etc [4-10]. Among them, doping of ZnO with Cd or Mg is interesting as these tend to improve its optical, electrical, morphological and structural properties. The band gap of ZnO is reduced by doping with cadmium and widens when doped with magnesium. There are a number of methods to prepare the doped ZnO thin films including physical and chemical deposition techniques such as sol gel processing [9], Chemical vapor deposition [11], Molecular beam epitaxy [12], spray pyrolysis [13], magnetron sputtering [14], pulsed laser deposition [15], electrochemical deposition [16] etc. Among these, sol gel processing is used as it has a number of advantages such as simple, economic, easily controlled and uniform structure formation.

There has been a lot of literature available for the magnesium and cadmium doped ZnO thin films, but the comparison for these under similar growth conditions is very rare. Therefore, we have systematically carried out the effect of Cd and Mg doping on the structural, morphological, optical and electrical properties of spin coated ZnO films by X-ray diffraction, Atomic force microscopy, UV-Vis spectroscopy, photoluminescence and resistivity measurement techniques.

2. Experimental details

The $Cd_{0.1}Zn_{0.9}O$ and $Mg_{0.1}Zn_{0.9}O$ thin films were deposited on alumina substrates by sol–gel route. The precursor chemicals, Zinc acetate dihydrate [$Zn(CH_3COO)_2.2H_2O$, CDH, 99.5%], Cadmium acetate dihydrate [$Cd(CH_3COO)_2.2H_2O$, SDFCI, 98%], Magnesium nitrate hexahydrate ($(Mg(NO_3)_2.6H_2O$, LobaChemie, 99%) and the ethanolamine [C_2H_7NO, Fisher Scientific, 98% pure] as sol stabilizer were used in the present synthesis. For depositing $Cd_{0.1}Zn_{0.9}O$(CZO) films, the calculated amounts of the precursors was used to form 0.2 M solution of zinc acetate dihydrate and cadmium acetate dehydrate in 10 ml solvent 2-ethoxyethanol with continuous stirring for an hour at 60°C. When the solution became transparent, the sol stabilizer ethanolamine was added in 1:1 molar ratio with zinc acetate and stirred for another one hour. Similar procedure has been followed to prepare $Mg_{0.1}Zn_{0.9}O$ (MZO) thin

films. These clear solutions were kept undisturbed for 24 h for necessary hydrolysis process. The aged sols were finally spun coated at 3000 rpm for 60 s by putting few drops on the well cleaned alumina substrates. Thereafter, the films were dried after each coating at preheating temperature ~250 °C in a hot air oven for 2 min. This process was repeated 15 times to obtain the dense films of appropriate thickness. The prepared thin films were then annealed at 600 °C in muffle furnace for one hour in air ambient.

The crystal phase structure was analysed with X'Pert PRO diffractometer (Panalytical, Germany) equipped with a Giono-meter PW3050/60 working with Cu K_α radiation (1.54060 Å). Surface morphology and dopant concentrations were obtained by scanning electron microscopy/energy-dispersive X-ray spectroscopy (SEM/EDS) (JEOL 6610 LV, JEOL Ltd., Akishima, Tokyo, Japan). The surface morphology of the films was analysed in contact mode by using atomic force microscope (Solver Pro-M4, NT-MDT, Russia). The two probe method is used to measure the electrical resistivity of the thin film samples. The optical transmittance spectrum was recorded with the help of UV–Vis spectrophotometer (Evolution 300, Thermo Scientific, USA). The excitation by 310 nm line of the xenon arc lamp was used to record the photoluminescence emission spectra at room temperature using the fluorescence spectrophotometer (Lambda 45, Perkin Elmer, USA).

3. Results and discussion

3.1 Structural characterization

Fig. 1 shows the X-ray diffraction patterns of the CZO and MZO nanostructured films annealed at 600° C. Both the samples show the preferential c-axis orientation perpendicular to the substrate with prominent diffraction peaks for (002) peak along with low intensity (100) and (101) peaks for the wurtzite-structured ZnO phase. However, the intensity of (002) diffraction peak is more dominant in MZO sample than for the CZO film, indicating a highly favourable c-axis orientation and crystalline structure. The absence of any peak related to the cubic CdO and MgO phase indicate that 10% doping of cadmium and magnesium does not affect the wurtzite phase of parent ZnO system and/or the films does not have any phase segregation or secondary phase formation.

The lattice parameters, 'a' and 'c' of the hexagonal wurtzite structured thin films can be calculated using the relations (1) and (2) given below [17, 18]:

$$a = \frac{2}{\sqrt{3}} d_{002} \quad (1)$$

$$c = 2d_{002} \quad (2)$$

where d is the interplanar spacing. For CZO film, the calculated values of lattice parameters 'a'=3.013Å and 'c'=5.219 Å while for MZO film, 'a'=3.002Å and 'c'=5.200Å which agrees with the JCPDS data. The average crystallite size has been evaluated using the well-known Debye–Scherrer formula as [19]:

$$D = \frac{0.9\lambda}{\beta cos\theta} \quad (3)$$

where β is the observed angular width at half maximum intensity (FWHM) of the peak; λ is the X-ray wavelength (1.5406 Å for Cu Kα) and θ is the Bragg's diffraction angle. The calculated crystallite size was found to be ~49.7 and 45.2 nm for the CZO and MZO films respectively.

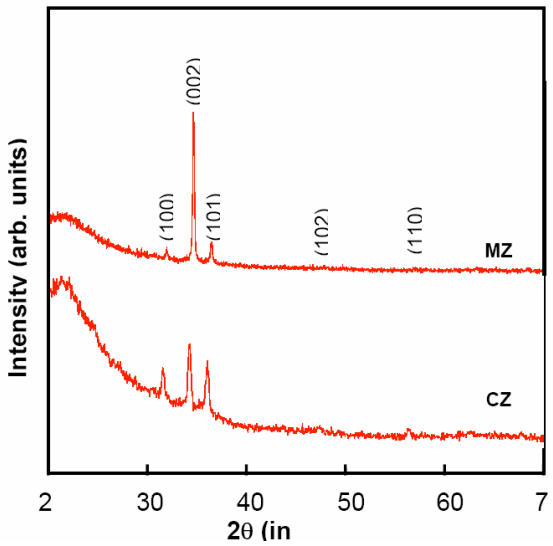

Fig. 1. X-ray diffraction patterns for the $Cd_{0.1}Zn_{0.9}O$ (CZO) and $Mg_{0.1}$ $Zn_{0.9}O$ (MZO) thin films.

The residual stress (σ) along the (002) diffraction plane has been calculated using the relation given below [18]:

$$\sigma = -233 \frac{(C_{film} - C_{bulk})}{C_{bulk}} \text{GPa} \quad (4)$$

where C_{bulk} is the lattice constants of standard ZnO powder (C_{bulk}= 5.205 nm) and C_{film} is the lattice constant of the deposited films. The negative values of stress ~ ⁻ 0.635 GPa, in CZO film due to the larger ionic size for the dopant Cd^{2+} (97 pm) for replacing the smaller ionic sized Zn^{2+} (72 pm) favour for the expansion of the lattice to yield the compressive stress. Similarly, the doping by the smaller ionic sized Mg^{2+} (66 pm) gives the stress ~ 0.231 GPa in the MZO film results in the tensile stress due to the contraction of the lattice. Also, the peak position for the (002) diffraction plane shifts toward higher angles with cadmium to magnesium dopant, indicating the relative change in the value of 'c' due to relatively larger and/or smaller sizes of the ionic radii of the dopants [20]. The peak position (P_{002}), FWHM of (002) plane (β_{002}), lattice parameters (a and c), residual stress (σ) and crystallite size (G_{XRD}) values for the CZO and MZO films are summarized in Table 1.

Table 1. Summary of parameters viz. the peak position, P_{002} and FWHM of (002) diffraction plane, Lattice parameters (a and c), Residual stress (σ) and Crystallite size (G_{XRD}) of the nanostructured films.

Sample	P_{002}	FWHM (rad.)	d-spacing (Å)	c (Å)	a (Å)	σ(GPa)	G_{XRD}(nm)
CZO	34.367	0.0029	2.610	5.219	3.013	-0.635	49.70
MZO	34.498	0.0032	2.600	5.200	3.002	0.231	45.21

3.2. Surface morphology

Fig. 2 shows the surface morphology (2D and 3D images) for the CZO and MZO films. The results show the formation of highly smooth surface morphology along with uniformly sized spherical grains in the MZO films while the higher surface roughness along with the random distribution of distorted spherical and cubical shaped grains for the CZO films. The calculated values of the grain size and surface roughness are 50.7 nm and 15.1 nm respectively for CZO film and 27.3 nm and 6.3 nm respectively for MZO film (Table 2). Thus, the grain size and surface roughness of the thin films is reduced as we change the dopant from cadmium to magnesium [21]. This may be due to the larger ionic size of Cd^{2+} than Zn^{2+} and hence cannot easily replace the zinc and favour the accumulation on the surface, giving rougher surface with large sized grains. On the other hand, the lower ionic sized Mg^{2+} easily replaced Zn^{2+} giving smoother surface with smaller grains.

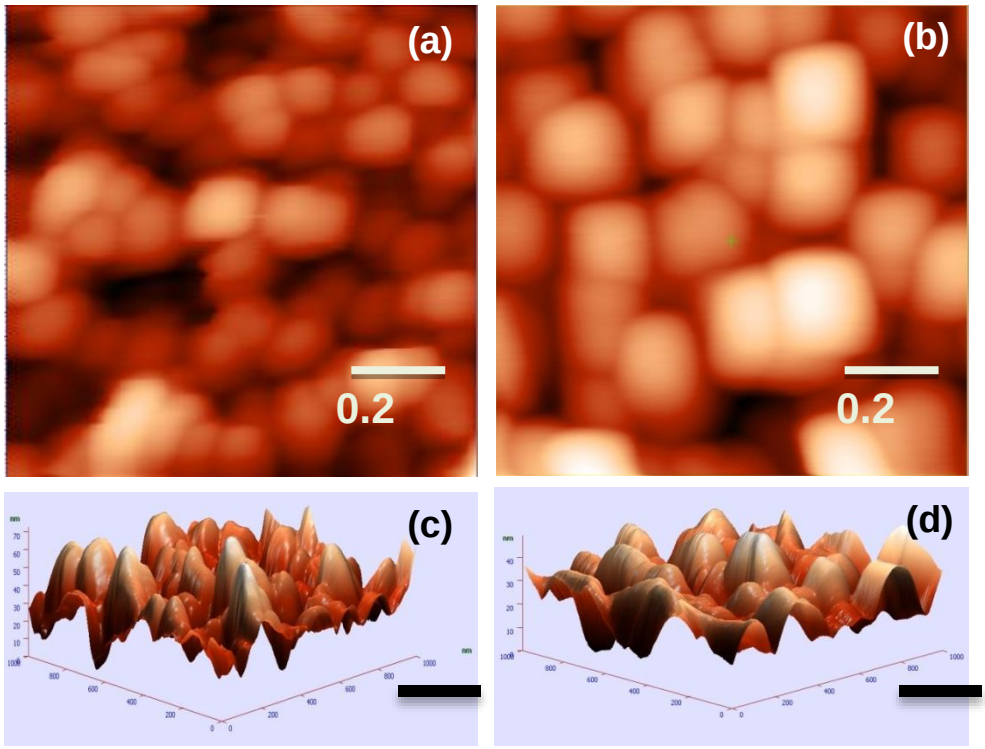

Fig. 2. 2D and 3D surface morphology of CZO films (a & c) and MZO films (b & d).

3.3. Optical properties

Fig. 3 shows the optical transmission spectra for CZO and MZO films in the wavelength range 200-1100 nm. Transmittance spectra of the films exhibit interference patterns with an average transmission more than 86% in the visible region indicating the good optical quality of the deposited films. The larger value of the optical transparency observed for the MZO film is because of its improved crystal structure and highly smooth surface,

which reduces the optically active surface defects in the prepared film. In the UV region, the CZO films show more transparency and may be used as UV photo-detectors. The absorption band edge shifts to shorter wavelengths (blue shift) with the change in dopant from cadmium to magnesium, indicating band gap broadening. From the transmission spectra, the absorption coefficient (α) is calculated using the following formula:

$$\alpha(\lambda) = \frac{1}{d} ln\left(\frac{1}{T}\right) \quad (5)$$

where d is the film thickness and T is the percentage transmittance of the films. The optical energy gap (E_g) and absorption coefficient (α) is related by the relation:

$$\alpha = \frac{C}{h\nu}\left((h\nu - E_g)^{\frac{1}{2}}\right) \quad (6)$$

which gives,

$$((\alpha h\nu)^2) = C(h\nu - E_g) \quad (7)$$

where, E_g is the direct optical band gap energy, hν is the incident photon energy, β=1/2 for direct band gap material ZnO and C is a constant [22]. The inset of Fig. 3 shows the variation of $(\alpha h\nu)^2$ versus photon energy (hν). The energy gap (E_g) of the samples is evaluated from the intercept of the linear portion of the each curve on x-axis [23]. It has been observed that the value of the optical gap is increased with the change in dopant type from Cd to Mg in the ZnO films.

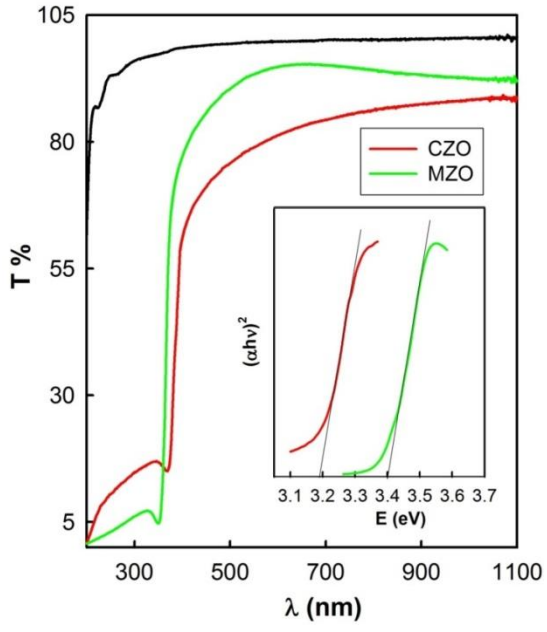

Fig. 3. Spectral dependence of the optical transmission for the CZO and MZO films(theblack line is for the bare alumina substrate). The inset picture shows the variation of $(\alpha h\nu)^2$ versus $h\nu$ for these films.

Fig. 4 shows the room temperature photoluminescence spectra of CZO and MZO films at 310 nm excitation energy. The value of the peaks in the emission spectrum for both the samples are summarised in Table 2. A strong dominant UV emission has been observed for both the samples associated to the intrinsic near band edge (NBE) emission and attributed to the recombination of free excitons through exciton-exciton collision process for the 3.37 eV (380 nm) wide direct band-gap transition of ZnO [24]. However, the peak position shifts toward shorter wavelength for the Mg dopant indicating the widening of the band gap [25]. The maximum intensity of this NBE peak may be attributed to higher density of free excitons for CZO sample. This emission in the near UV region confirms a good crystal structure of the prepared samples.

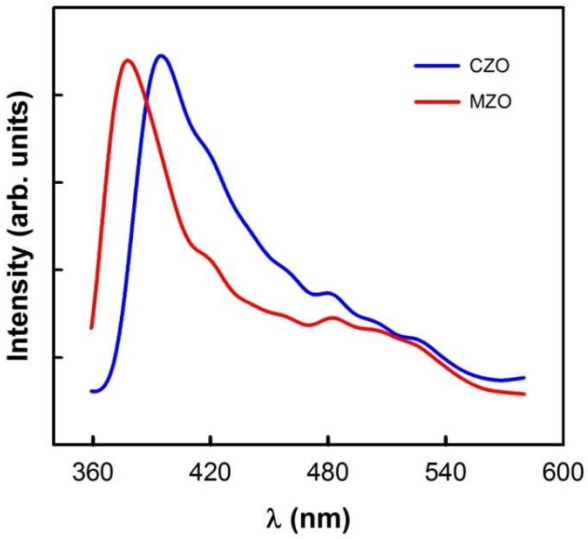

Fig. 4. Photoluminescence emission spectra for the CZO and MZO films at 310 nm excitation energy.

Two low intensity peaks at 420 nm and 485 nm has also been observed, which indicates blue emission by the prepared samples. This blue emission is attributed to oxygen related defects (oxygen vacancies or oxygen interstitials), which are more dominating in CZO film. A small intensity green emission peak centred at 527 nm for sample CZO is also being observed attributed to the deep level defects such as zinc vacancy or oxygen vacancy in ZnO, which is being created due to the evaporation of oxygen with the annealing of the sample at 600 ^{0}C [25]. Similar value of the optical gap was also reported for Cd doped ZnO films by spray pyrolysis technique by Moghe et al. [26]. These donor oxygen vacancies should drag the Fermi level towards the conduction band. Hence the oxygen vacancies created in lattice structure. However, this peak is not broad indicating least porous films structure [27]. The optical gap (E_g) and PL peak positions are summarised in the Table 2.

Table 2. Summary of various parameters viz. grain size (D_{AFM}), RMS surface roughness (Sq), optical band gap (E_g) and PL peaks of CZO and MZO films.

Sample	$\mathbf{D_{AFM}}$ (nm)	**Sq**(nm)	$\mathbf{E_g}$ (eV)	**PL peaks**(nm)			
				I^{st}	II^{nd}	III^{rd}	IV^{th}
CZO	50.7	15.1	3.18	394	419.5	482.5	527
MZO	27.3	06.3	3.40	378	420.0	483.5	524

3.4. Electrical properties

Ambient temperature resistivity of the thin films prepared under the same conditions shows that the electrical resistivity of the sample CZO is 24.6 Ω-cm and for sample MZO is 16944 Ω-cm (Table 2). This high resistivity in MZO may be due reason that when Mg is doped into ZnO, interstitial metal atom and oxygen vacancies can be depressed, which however make our material a p-type or n-type semiconductor [28].There is also the possibility that a spot of Mg at the grain boundaries may produce electrical barriers, increasing scattering of the carriers, and thus increase the resistivity [29]. On the other hand, low electrical resistivity is being observed for CZO film [30, 31].

4. Conclusions

We have successfully prepared the CZO and MZO films by spin coating technique on the alumina substrates. The XRD studies confirms the preferred c-axis orientated hexagonal wurtzite structure along with the observation of compressive and tensile stresses for the Cd and Mg doped ZnO films respectively. The smaller grains and highly smooth surface has been observed for the MZO films as compared to the CZO films. The MZO films have found to exhibit larger value of average optical transparency (>93%) as compared to the CZO films (<86%). The optical band gap is found to be 3.18 eV and 3.40 eV for CZO and MZO respectively. The photoluminescence spectra show the blue shift of the near band edge emission peak for the MZO films as compared to the CZO films due to the band gap widening. Both the samples exhibit the blue light emission indicating the presence of oxygen related defects. MZO film is highly resistive whereas CZO film is highly conductive. These results reveal that the doping of Mg in ZnO is found to influence greatly its structure, morphology, optical and electrical properties specifically in low wavelength side due to its wide band gap.

Acknowledgements

The authors are thankful Dr. Rajiv Kumar for the optical spectroscopy of our samples and Prof. R. Thangaraj for helpful suggestions.

References

[1] C. Tsay, H. Cheng, Y. Tung, W. Tuan, C. Lin, Thin Sol. Films **517**, 1032 (2008).
[2] Z. Tang, G. Wong,P. Yu, M. Kawasaki,A. Ohtomo, H. Koinuma, Y. Segawa,Appl. Phys. Lett. **72**(25), 3270 (1998).
[3] H. Bahadur, A. Srivastava, S. Garg, P. Lal, S. Chandra,IEEE 0-7803-9052, 146 (2005).
[4] Y. Caglar, M. Caglar, S. Ilican, A. Ates,J. Phys. D: Appl. Phys. **42**, 065421 (2009).
[5] M. Vishwasa, R. K. Narasimha, A. R. Phani, K. V. Arjuna, R. P. Chakradhar, Sol. Stat. Comm. **152**, 324 (2012).
[6] A. Srivastava, J. Kumar, AIP Adv. **1**(032153), 1-10 (2011).
[7] Y. Ke, J. Berry, P. Parilla, A. Zakutayev, R. O'Hayre, D. Ginley, Thin Solid Films **520**, 3697 (2012).
[8] S. Aksoy, Y. Caglar, S. Ilican, M. Caglar, OpticaApplicata, **XL**(1), 7 (2010).
[9] M. Rokn-Abadi, M. Behdani, H. Arabshahi, N. Hosseini,Int. Rev. Phys. **12**, 3 (2009).
[10] L. Wang, L. Meng, V. Teixeira, S. Song, Z. Xu, X. Xu,Thin Solid Films **517**, 3721 (2009).
[11] J. Ye, S. Gu, S. Zhu, T. Chen, L. Hu, F. Qin, R. Zhang, Y. Shi, Y. Zheng,J.Cryst. Growth **243**(1), 151 (2002).
[12] S. Sadovef,S. Blumstengel, J. Cui, J. Puls, S. Rogaschewski, P. Schafer, Appl. Phys. Lett. **89**, 201907 (2006).
[3] C. Muiva, T. Sathiaraj, K. Maabong, Ceram. Internat. **37**, 555 (2011).
[14] J. Lee, S. Kwak,H. Kim,Thin Solid Films **423**(2), 262 (2003).
[15] V. R. Kumar, K. J. Lethy,A. Kumar, R. Krishnan, N. V. Pillai, V. P. M. Pillai, R. Philip, Mater. Chem. Phys. **121**, 406 (2010).

[16] T. Singh, D. K. Pandya, R. Singh, J. All. Compd. **509**, 5095 (2011).
[17] M. Khanlary, S. Isazadeh, Micro Nano Lett. **6**(9), 767 (2011).
[18] A. Singh, P. Kumar,Int. Nano Lett. 3, 57 (2013)
[19] K. Anand, P. Kumar, R. Thangaraj, J. Optoelectron. Adv. Mater. **13**(6), 702 (2011).
[20] S. Vijayalakshmi, S. Venkataraj, R. Jayavel, J. Phys. D: Appl. Phys.**41**, 245403 (2008).
[21] R. Ding, R. Xu, B. Gu, Z. Shi, H. Wang, L. Ba, Z. Xiao, J. Mater. Sci. Technol. **26**(7), 601 (2010).
[22] L. B. Duan, X. R. Zhao, J. M. Liu, W. C. Geng, H. Y. Xie, H. N. Sun,Phys. Scr. **85**, 035709 (2012).
[23] P. Kumar, R. Thangaraj, T. S. Sathiaraj, Phys. Stat. Solidi A **208**(4), 838 (2011).
[24] N. Gayen, K. Sarkar, S. Hussain, R. Bhar, A. Pal, Ind. J. Pure Appl. Phys. **49**, 470 (2011).
[25] A. Singh, D. Kumar, P. K. Khanna, A. Kumar, M. Kumar, M. Kumar, Thin SolidFilms **519**, 58260 (2011).
[26] S. Moghe, R. Panda, S.B. Shrivastawa, M. Gangrade, T. Shripathi, D.M. Phase, V. Ganeshan, Thin Solid Films **525**, 49 (2012).
[27] F. Ghodsi, H. Absalan, Acta Phys. Polo. A **118**(4), 659 (2010).
[28] C. Tsay, M. Wang, S. Chiang, Mater. Trans. **49**(5), 1186 (2008).
[29] K. Huang, Z. Tang, L. Zhang, J. Yu, J. Lv, X. Liu, F. Liu, Appl. Surf. Sci. **258**, 3710 (2012).
[30] H. Tabet-Derraz, N. Benramdane, D. Nacer, A. Bouzidi, M. Medles, Sol.Ener. Mater. Sol. Cells **73**, 249 (2002).
[31] Y. Choi, C. Lee, S. Cho, Thin Solid Films **289**(1-2), 153 (1996).

*Corresponding author: prafiziks@gmail.com